Fizika Nizkikh Temperatur, 2002, v. 28, No. 7 , p. 752–762

# Electronic excitations and correlations in quantum bars

I. Kuzmenko, S. Gredeskul, K. Kikoin, and Y. Avishai

*Department of Physics, Ben-Gurion University of the Negev, P.O.Box 84105 Beer-Sheva, Israel*
E-mail: sergeyg@bgumail.bgu.ac.il

Received February 1, 2002

The spectrum of boson fields and two-point correlators are analyzed in a quantum bar system (a superlattice formed by two crossed interacting arrays of quantum wires), with a short-range interwire interaction. The standard bosonization procedure is shown to be valid, within the two-wave approximation. The system behaves as a sliding Luttinger liquid in the vicinity of the Γ point, but its spectral and correlation characteristics have either 1D or 2D nature depending on the direction of the wave vector in the rest of the Brillouin zone. Due to the interwire interaction, unperturbed states propagating along the two arrays of wires are always mixed, and the transverse components of the correlation functions do not vanish. This mixing is especially strong around the diagonals of the Brillouin zone, where the transverse correlators have the same order of magnitude as the longitudinal ones.

PACS: **73.23.–b**, **73.40.–c**

## 1. Introduction

Diverse $D-1$ dimensional objects embedded in $D$-dimensional structures were recently investigated experimentally and analysed theoretically. Rubbers and various percolation networks are examples of such disordered $D-1$ objects, whereas self-organized stripes in oxicuprates, manganites, nanotube ropes, and quantum Hall systems are examples of ordered (periodic) structures of this kind. In some cases, the effective dimensions of such structures may be intermediate, e.g., between $D=1$ and $D=2$. They are especially promising candidates for studying novel electronic correlation properties, which, in particular, are relevant for the search of Luttinger liquid (LL) fingerprints in two dimensions. This challenging idea is motivated by noticing some unusual properties of electrons in Cu–O planes in high-$T_c$ materials [1]. However, the Fermi liquid state seems to be rather robust in two dimensions. In this respect, a 2D system of weakly coupled 1D quantum wires [2–4] looks promising. Indeed, a theoretical analysis of stable LL phases was recently presented for a system consisting of coupled parallel quantum wires [5–7] and for 3D stacks of sheets of such wires in parallel and crossed orientations [8]. In most of these cases, the interaction between the parallel quantum wires is assumed to be perfect along the wire [8], whereas the interaction between the modes generated in different wires depends only on the interwire distance. Along these lines, generalization of the LL theory for quasi-2D (and even 3D) systems is reported in Ref. 8, where the interaction between two crossed arrays of parallel quantum wires forming some kind of a network depends on the distance between points belonging to different arrays. As a result, the grid of crossed arrays retains its LL properties for propagation along both subsets of parallel wires, whereas the cross-correlations remain nonsingular. This LL structure can be interpreted as a quantum analog of a classical sliding phases of coupled $XY$ chains [9]. A special case of 2D grid where the crossed wires are coupled by tunneling interaction is considered in Refs. 4, 10.

In the present paper, a different course is elaborated. We ask the question of whether it is possible to encode *both 1D and 2D electron liquid regimes in the same system within the same energy scale.* In order to unravel the pertinent physics we consider a grid with *a short-range capacitive interwire interaction.* This approximation might look shaky if applied for crossed stripe arrays in the cuprates. On the other hand, it seems natural for 2D grids of

nanotubes [11,12] or artificially fabricated bars of quantum wires with grid periods $a_{1,2}$ which exceed the lattice spacing of a single wire or the diameter of a nanotube. It will be shown below that this interaction can be made effectively weak. Therefore, such a quantum bars (QB) retain the 1D LL character for the motion along the wires, similarly to the case considered in Ref. 8. At the same time, however, boson mode propagation along the diagonals of the grid is also feasible. This process is essentially a two-dimensional one, as are the shape of the Brillouin zone and equipotential surfaces in the reciprocal QB lattice.

Before developing the formalism, a few words about the main assumptions are in order. Our attention here is mainly focused on charge modes, so it is assumed that there is a gap for spin excitations. Next, we are mainly interested in electronic properties of QBs which are not related to simple charge instabilities like commensurate CDWs, so that the (for simplicity equal) periods $a_1 = a_2 = a$ are supposed to be incommensurate with the lattice spacing. The Brillouin zone (BZ) of the QB superlattice is two-dimensional, and the nature of excitations propagating in this BZ is determined by Bragg interference of modes with the superlattice wave vector. This interference (umklapp processes) is, of course destructive for LL excitations with both wave vector components close to multiple integers of $Q \equiv 2\pi/a$. However, in case of weak scattering, only two-wave interference processes near the boundaries of the BZ are significant. One can then hope that the harmonic boson modes survive in the major part of the BZ, and that the Hamiltonian of the QB might still be diagonalized without losing the main characteristic features of the LL physics.

## 2. Quantum bars: basic notions

Quantum bars may be defined as a 2D periodic grid, i.e., two crossed periodic arrays of 1D quantum wires with a period $\mathbf{a} = (a_1, a_2)$. In fact these arrays are placed on two parallel planes separated by an interplane distance [12], but in this section we consider QB as a genuine 2D system. The arrays are oriented along the unit vectors $\mathbf{e}_{1,2}$ with an angle $\varphi$ between them. Here we consider a square grid ($\varphi = \pi/2$) formed by identical wires of length $L$ with basis vectors $\mathbf{a}_j = a\mathbf{e}_j$, $j = 1, 2$ (Fig. 1). The interaction between the excitations in different wires is assumed to be concentrated near the crossing points with coordinates $n_1\mathbf{a}_1 + n_2\mathbf{a}_2 \equiv (n_1 a, n_2 a)$. The integers $n_j$ enumerate the wires within the $j$th array. Such interaction imposes a superperiodicity on the energy spectrum of initially one-dimensional quantum wires, and the eigenstates of this superlattice are characterized by a 2D quasimomentum $\mathbf{q} = q_1\mathbf{g}_1 + q_2\mathbf{g}_2 \equiv (q_1, q_2)$. Here $\mathbf{g}_{1,2}$ are the unit vectors of the reciprocal superlattice satisfying the standard orthogonality relations $(\mathbf{e}_i \cdot \mathbf{g}_j) = \delta_{ij}$. The corresponding basis vectors of the reciprocal superlattice have the form $(m_1 Q, m_2 Q)$, where $Q = 2\pi/a$ and $m_{1,2}$ are integers.

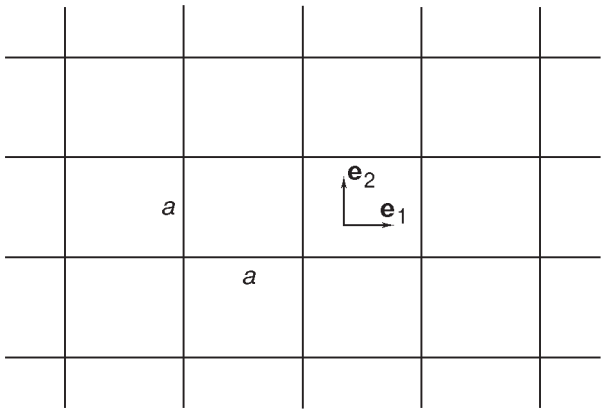


*Fig. 1.* Square quantum bars formed by two interacting arrays of parallel quantum wires. $\mathbf{e}_1$, $\mathbf{e}_2$ are the unit vectors of the superlattice.

In conventional 2D systems, forbidden states in reciprocal space arise due to Bragg diffraction in a periodic potential, whereas the whole plane is allowed for wave propagation in real space, at least till the periodic potential is weak enough. In sharply anisotropic QBs most of the real space is forbidden for electron and plasmon propagation, whereas the Bragg conditions for the wave vectors are still the same as in conventional 2D plane modulated by a periodic potential. The excitation motion in QBs is one-dimensional in the major part of the 2D plane, and the anisotropy in real space imposes restrictions on the possible values of the 2D coordinates $\mathbf{x} = (x_1, x_2)$. At least one of them, e.g., $x_2$ should be an integer multiple of the interwire distance $a$, so that the coordinate $\mathbf{x} = (x_1, n_2 a)$ characterizes the point with the 1D coordinate $x_1$ lying at the $n_2$-th wire of the first array.

The 2D Brillouin zone of a QB is constructed as an extension of the 1D Brillouin zones of two crossed arrays and subsequent folding of this BZ in accordance with the square superstructure. However, one cannot resort to the standard basis of 2D plane waves when constructing the eigenstate with a given wave vector $\mathbf{k}$ in the BZ because of the kinematic restrictions mentioned above. Even in *non-interacting* arrays of quantum wires the 2D basis is formed as a superposition of two sets of 1D waves.

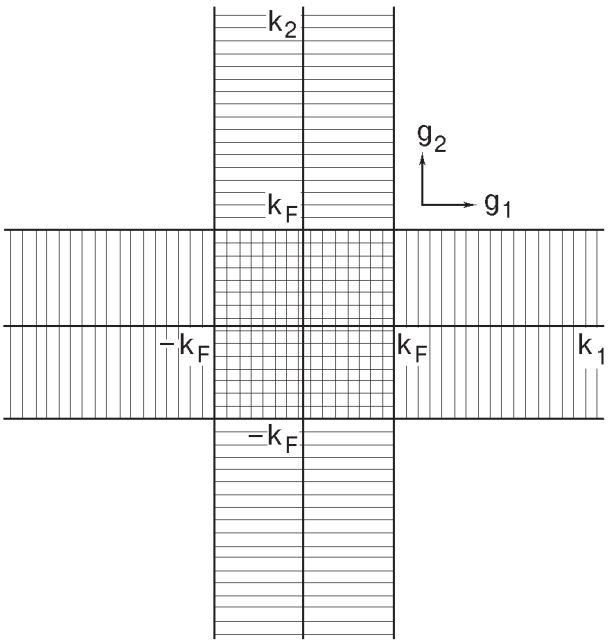


*Fig. 2*. Fermi surface of square metallic quantum bars in the absence of charge transfer between wires. $\mathbf{g}_1$ , $\mathbf{g}_2$ are the unit vectors of the reciprocal superlattice.

The first of them is a set of 1D excitations propagating along *each* wire of the first array characterized by a unit vector $k_1\mathbf{e}_1$ with a phase shift $ak_2$ between adjacent wires. The second set is the similar manifold of excitations propagating along the wires of the second array with a wave vector $k_2\mathbf{e}_2$ and phase shift $ak_2$ . The states of equal energy obtained by means of this procedure form straight lines in the 2D BZ. For example, the QB Fermi surface developed from the points $\pm k_F$ for an individual quantum wire consists of two sets of lines $|k_{1,2}| = k_F$ . Accordingly, the Fermi sea is not a circle with radius $k_F$ like in the case of free 2D gas, but a cross in the $k$ plane bounded by these four lines [4] (see Fig. 2). Of course, these equipotential lines describe the 1D excitations in the BZ of a QB.

Due to weakness of the interwire interaction, the excitations in the 2D BZ depicted in Fig. 3 acquire genuine two-dimensionality characterized by the quasimomentum $\mathbf{q} = (q_1, q_2)$. However, in case of weak interaction the 2D waves constructed from the 1D plane waves in accordance with the above procedure form an appropriate basis for the description of elementary excitations in QB in close analogy with the nearly free electron approximation in conventional crystalline lattices. It is easily foreknown that the interwire interaction does not completely destroy the above quasimomentum classification of eigenstates, and the 2D reconstruction

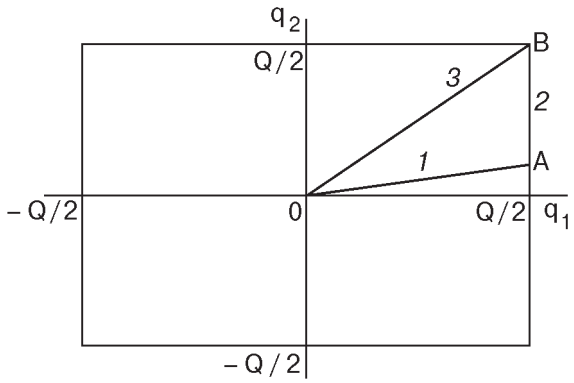


*Fig. 3*. Two dimensional Brillouin zone of a square QB. The three directions along which the dispersion of Bose excitations is calculated in Sec. 5 are marked by the indices *1*, *2*, *3*.

of the spectrum may be described in terms of wave mixing similarly to the standard Bragg diffraction in a weak periodic potential. Moreover, the classification of eigenstates of noninteracting crossed arrays of 1D wires («empty superlattice») may be effectively used for the classification of energy bands in a real QB superlattice. Our next step is to construct a complete 2D basis for this empty superlattice.

Due to LL nature of the excitations in a given wire, they are described as plane waves $L^{-1/2}\exp(ikx)$ with wave number $k$ and initial dispersion law $\omega_0(k) = v|k|$. Each excitation in a corresponding «empty superchain» is described by its quasi-wavenumber $q$ and the band number $p$ ($p = 1, 2, \ldots$). Its wave function has the Bloch-type structure

$$\psi_{p,q}(x) = \frac{1}{\sqrt{L}} e^{iqx} u_{p,q}(x) \qquad (1)$$

with the Bloch amplitude

$$u_{p,q}(x) = \sum_{n=-\infty}^{\infty} \frac{\sin\xi_n}{\xi_n} \times$$

$$\times \cos[(2p-1)\xi_n] \exp\left(-4i\xi_n \frac{q}{Q}\right),$$

$$\xi_n = \frac{\pi}{2}\left(\frac{x}{a} - n\right).$$

The corresponding dispersion law $\omega_p(q)$ has the form

$$(vQ)^{-1}\omega_p(q) = \frac{2p-1}{4} +$$

$$+\sum_{n=1}^{\infty}\frac{2(-1)^p}{\pi^2(2n+1)^2}\cos\frac{2\pi(2n+1)}{Q}\,.$$

Within the first BZ of a superchain, $|q|\le Q/2$, expressions for the Bloch amplitude and dispersion law are substantially simplified:

$$u_{p,q}(x)=\exp\left\{iQx(-1)^{p-1}\left[\frac{p}{2}\right]\operatorname{sgn}q\right\}, \qquad (2)$$

$$\omega_p(q)=vQ\left(\left[\frac{p}{2}\right]+(-1)^{p-1}\frac{|q|}{Q}\right). \qquad (3)$$

The 2D basis of periodic Bloch functions for an empty superlattice is constructed in terms of the 1D Bloch functions (1), (2):

$$\Psi_{p,p',\mathbf{q}}(\mathbf{r})=\psi_{p,q_1}(x_1)\psi_{p',q_2}(x_2)\,. \qquad (4)$$

Here $p, p'=1, 2, \ldots$, are the band numbers and the 2D quasimomentum $\mathbf{q}=(q_1, q_2)$ belongs to the first BZ, $|q_j|\le Q/2$. The corresponding eigenfrequencies are

$$\omega_{pp'}(\mathbf{q})=\omega_p(q_1)+\omega_{p'}(q_2)\,. \qquad (5)$$

We will use this basis in the next Section when constructing the excitation spectrum of QBs within the reduced band scheme.

### 3. Hamiltonian

The full Hamiltonian of the QBs is

$$H=H_1+H_2+H_{\rm int}\,, \qquad (6)$$

where $H_j$ describes the 1D boson field in the $j$th array

$$H_1=\frac{\hbar v}{2}\sum_{n_2}\int_{-L/2}^{L/2}dx_1\left\{g\pi_1^2(x_1, n_2a)+\frac{1}{g}(\partial_{x_1}\theta_1(x_1, n_2a))^2\right\},$$

$$H_2=\frac{\hbar v}{2}\sum_{n_1}\int_{-L/2}^{L/2}dx_2\left\{g\pi_2^2(n_1a, x_2)+\frac{1}{g}(\partial_{x_2}\theta_2(n_1a, x_2))^2\right\},$$

and $(\theta_j, \pi_j)$ are the conventional canonically conjugate boson fields (see, e.g., Ref. 13). The Fermi velocities $v_{1,2}=v$ and the LL parameters $g_{1,2}=g$ are taken to be the same for both arrays. Generalization to the case of different parameters $v_j$, $g_j$, $a_j$ is straightforward.

The interwire interaction results from a short-range contact capacitive coupling in the crosses of the bar,

$$H_{\rm int}=\sum_{n_1,n_2}\int_{-L/2}^{L/2}dx_1dx_2V(x_1-n_1a, n_2a-x_2)\times$$

$$\times\rho_1(x_1, n_2a)\rho_2(n_1a, x_2)\,.$$

Here $\rho_i(\mathbf{r})$ are density operators, and $V(\mathbf{r}_1-\mathbf{r}_2)$ is a short-range interwire interaction. Physically, it represents the Coulomb interaction between charge fluctuations $e\varsigma(x/r_0)$, $\varsigma(0)=1$ around the points $\mathbf{r}_1=(x_1, n_2a)$ and $\mathbf{r}_2=(n_1a, x_2)$. The size of these fluctuations is determined by the screening radius $r_0$ within the wire. One may neglect the interwire tunneling and restrict oneself to the capacitive interaction only, provided the vertical distance between the wires $d$ is substantially larger than the screening radius $r_0$. Therefore the interaction has the form

$$V(\mathbf{r})=\frac{V_0}{2}\Phi\left(\frac{x_1}{r_0}, \frac{x_2}{r_0}\right),$$

where the function $\Phi(\xi_1, \xi_2)$ is

$$\Phi(\xi_1, \xi_2)=\frac{\varsigma(\xi_1)\varsigma(\xi_2)}{\sqrt{1+\left(\frac{r_0}{d}\right)^2(\xi_1^2+\xi_2^2)}}\,. \qquad (7)$$

It is seen from these equations that $\Phi(\xi_1, \xi_2)$ is an even function of its arguments; it vanishes for $|\xi_{1,2}|\ge 1$ and is normalized by condition $\Phi(0,0)=1$. The effective coupling strength is

$$V_0=\frac{2e^2}{d}\,.$$

In terms of boson field operators $\theta_i$, the interaction is written as

$$H_{\rm int}=V_0\sum_{n_1,n_2}\int_{-L/2}^{L/2}dx_1dx_2\Phi\left(\frac{x_1-n_1a}{r_0}, \frac{n_2a-x_2}{r_0}\right)\times$$

$$\times\partial_{x_1}\theta_1(x_1, n_2a)\partial_{x_2}\theta_2(n_2a, x_2)\,.$$

In the quasimomentum representation (4), (1), (2) the full Hamiltonian (6) acquires the form

$$H=\frac{\hbar vg}{2a}\sum_{j=1}^{2}\sum_{p}\sum_{\mathbf{q}}\pi^+_{jp\mathbf{q}}\pi_{jp\mathbf{q}}+$$

$$+\frac{\hbar}{2vga}\sum_{jj'=1}^{2}\sum_{pp'}\sum_{\mathbf{q}}W_{jpj'p'\mathbf{q}}\theta^+_{jp\mathbf{q}}\theta_{j'p'\mathbf{q}} \qquad (8)$$

with matrix elements for interwire coupling given by

$$W_{jpj'p'\mathbf{q}} = \omega_{jp\mathbf{q}}\omega_{j'p'\mathbf{q}}[\delta_{jj'}\delta_{pp'} + \phi_{jpj'p'\mathbf{q}}(1-\delta_{jj'})] .$$

Here

$$\omega_{jp\mathbf{q}} \equiv \omega_p(q_j) = v\left(\left[\frac{p}{2}\right]Q + (-1)^{p+1}|q_j|\right) \quad (9)$$

are eigenfrequencies (3) of the «unperturbed» 1D mode pertaining to an array $j$, band $p$, and quasimomentum $q_j\mathbf{g}_j$ . The coefficients

$$\phi_{jpj'p'\mathbf{q}} = \phi(-1)^{p+p'}\,\mathrm{sgn}\,(q_1q_2)\,\Phi_{jpj'p'\mathbf{q}}$$

$$\phi = \frac{gV_0r_0^2}{\hbar v a} \quad (10)$$

are proportional to the dimensionless Fourier component of the interaction strengths,

$$\Phi_{1p2p'\mathbf{q}} = \int d\xi_1 d\xi_2 \Phi(\xi_1,\xi_2)\mathrm{e}^{-i\eta_0(q_1\xi_1+q_2\xi_2)} \times$$

$$\times\, u^*_{p,q_1}(r_0\xi_1)u^*_{p',q_2}(r_0\xi_2) = \Phi_{2p'1p\mathbf{q}}. \quad (11)$$

The Hamiltonian (8) describes a system of coupled harmonic oscillators, which can be exactly diagonalized with the help of a certain canonical linear transformation (note that it is already diagonal with respect to the quasimomentum $\mathbf{q}$). The diagonalization procedure is, nevertheless, rather cumbersome due to the mixing of states belonging to different bands and arrays. However, it will be shown below that the dimensionless interaction parameter $\phi$ (10) is effectively weak, and a perturbation approach is applicable.

## 4. Main approximations

As was mentioned in the Introduction, we consider rarefied QBs with a short-range capacitive interaction. In the case of QBs formed by nanotubes, this is a Coulomb interaction screened at a distance of the order of the nanotube radius [14] $R_0$ , and therefore $r_0 \sim R_0$ . The minimal radius of a single-wall carbon nanotube is about $R_0 =$ = 0.35–0.4 nm (see Ref. 15). The intertube vertical distance $d$ in artificially produced nanotube networks is estimated as $d \approx 2$ nm [12]. Therefore the dimensionless interaction $\phi$ (10) can be estimated as

$$\phi \sim \sqrt{\varepsilon}\,\frac{R_0}{a} , \quad (12)$$

where

$$\sqrt{\varepsilon} = \frac{2R_0}{d}\,\frac{ge^2}{\hbar v} . \quad (13)$$

The first factor is about 0.35. The second one, which is nothing but the «fine structure» constant for the nanotube QBs, can be estimated as 0.9 (we used the values $d = 1/3$ and $v = 8\cdot 10^7$ cm/s [11]). Therefore $\varepsilon$ is approximately equal to 0.1. The modulus of the matrix element (11) with the exponential form of $\varsigma(\xi) = \exp(-|\xi|)$ does not exceed unity, so that the interaction (11) is really weak.

The smallness of dimensionless interaction $\phi$ enables one to apply perturbation theory. In this limit, the systematics of unperturbed levels and states is grossly conserved, at least in the low-energy region corresponding to the first few bands. This means that they should be described by the same quantum numbers (array number, band number, and quasimomentum). Indeed, as follows from the unperturbed dispersion law (9), the interband mixing is significant only along the high-symmetry directions in the first BZ (BZ boundaries and lines $g_i = 0$). In the rest of the BZ this mixing can be taken into account perturbatively. The interarray mixing within the same energy band is strong for waves with quasimomenta close to the diagonal of the BZ. Away from the diagonal, it can also be calculated perturbatively.

For quasimomenta far from the BZ diagonals and high-symmetry directions, and in second order of perturbation theory, the above-mentioned canonical transformation results in the following renormalized field operators for the first array:

$$\tilde{\theta}_{1p\mathbf{q}} = \left(1 - \frac{1}{2}\beta_{p\mathbf{q}}\right)\theta_{1p\mathbf{q}} + \sum_{p'}\phi_{pp'\mathbf{q}}\theta_{2p'\mathbf{q}}, \quad (14)$$

where

$$\phi_{pp'\mathbf{q}} = \frac{\phi_{1p2p'\mathbf{q}}\omega_{1p\mathbf{q}}\omega_{2p'\mathbf{q}}}{\omega^2_{1p\mathbf{q}} - \omega^2_{2p'\mathbf{q}}}$$

and

$$\beta_{p\mathbf{q}} = \sum_{p'}\phi^2_{pp'\mathbf{q}} . \quad (15)$$

Below, the specific values of these coefficients

$$\phi_{p\mathbf{q}} \equiv \phi_{1p\mathbf{q}}, \quad (16)$$

$$\phi_{\mathbf{q}} \equiv \phi_{1\mathbf{q}} \equiv \phi_{11\mathbf{q}}, \quad (17)$$

$$\beta'_{p\mathbf{q}} = \sum_{p'\neq p}\phi^2_{pp'\mathbf{q}} \quad (18)$$

will also be used. The renormalized eigenfrequencies for the first array are

$$\tilde{\omega}^2_{1p\mathbf{q}} = \omega^2_{1p\mathbf{q}}\left(1 + \sum_{p'}\gamma_{pp'\mathbf{q}}\right), \qquad (19)$$

where

$$\gamma_{pp'\mathbf{q}} = \frac{\phi^2_{1p2p'\mathbf{q}}\omega^2_{2p'\mathbf{q}}}{\omega^2_{1p\mathbf{q}} - \omega^2_{2p'\mathbf{q}}}\,.$$

Corresponding formulas for the second array are obtained by replacing $1p \to 2p$, and $1p' \to 2p'$.

Consider now the frequency correction in Eq. (19) more attentively. In the case under consideration, all terms in Eq. (19) are nonsingular. Then, away from the BZ boundary ($|\mathbf{q}| << Q/2$) the following estimate is valid:

$$\frac{\omega^2_{jp\mathbf{q}}}{\omega^2_{jp\mathbf{q}} - \omega^2_{j'1\mathbf{q}}} \approx 1 + O\left(\frac{q^2_{j'}}{(pQ)^2}\right),$$

$$(j,\, j') = (1,\, 2),(2,\, 1); \quad p > 1.$$

Therefore, the correction term can be estimated approximately as $\omega^2_{11\mathbf{q}} S_{\mathbf{q}}$, with

$$S_{\mathbf{q}} = \sum_p \phi^2_{112p\mathbf{q}} = \varepsilon\,\frac{R_0^2}{a^2}\sum_p \Phi^2_{112p\mathbf{q}}. \qquad (20)$$

Due to the short-range character of the interaction, the matrix elements $\Phi_{112p\mathbf{q}}$ vary slowly with band number, being of the order of unity for $p < p_{\max} \sim a/R_0$, and decrease rapidly for $p > p_{\max}$. Therefore, the right-hand side in Eq. (20) can roughly be estimated as

$$S_{\mathbf{q}} \sim \varepsilon\,\frac{R_0}{a} = 0.1\,\frac{R_0}{a} << 1\,. \qquad (21)$$

One should also remember that the energy spectrum of nanotube remains one-dimensional only for frequences smaller than some $\omega_m$. Therefore, an external cutoff arises at $p = ak_m$, where $k_m \sim \omega_m/v$. As a result, one gets the estimate

$$S_{\mathbf{q}} \sim \varepsilon\,\frac{R_0}{a}\,k_m R_0\,. \qquad (22)$$

Hence, one could hope to gain here an additional power of the small interaction radius, but for nanotubes, $k_m$ is of the order of $1/R_0$ (see Refs. 16, 11) and the two estimates coincide.

For quasimomenta close to the BZ center, the coefficient $S_{\mathbf{q}}$ can be calculated exactly. Due to smoothness of the matrix elements $\phi_{112p\mathbf{q}}$ with respect to the band number $p$, the sum over $p$ in Eq. (20) can be replaced by an integral over the extended BZ with wave vector $\mathbf{k}$ whose components are

$$k_j = q_j + \mathrm{sgn}(q_j)(-1)^{p_j+1}[p_j/2]Q. \qquad (23)$$

For $|\mathbf{q}| \le Q/2$ one gets $|S_{\mathbf{q}}| \le |S_0|$, where

$$S_0 = \frac{\varepsilon R_0^2}{2\pi a}\int_{-\infty}^{\infty} dk\,\Phi^2(k)$$

and

$$\Phi(k) = \int d\xi_1 d\xi_2 \Phi(\xi_1, \xi_2)\,\mathrm{e}^{-ik\xi_2}.$$

Finally, one obtains

$$S_0 = \varepsilon\Phi_0^2\,\frac{R_0}{a}\,, \qquad (24)$$

where the constant

$$\Phi_0^2 = \int d\xi d\xi_1 d\xi_2 \Phi(\xi_1, \xi)\Phi(\xi_2, \xi)$$

for the exponential form of $\varsigma(\xi) \propto \exp\left(-|\xi|\right)$ is $\approx 1.5$. As a result, instead of the preliminary estimate (21), we have

$$S_0 = 0.14\,\frac{R_0}{a}\,.$$

Thus the correction term in Eq. (19) is in fact small.

## 5. Energy spectrum

In the major part of the BZ, for quasimomenta $\mathbf{q}$ lying far from the diagonal, the spectrum is described by Eqs. (14), (19). Here each eigenstate (14) mostly conserves its initial systematics, i.e., belongs to a given array, and mostly depends on a given quasimomentum component. The corresponding dispersion laws (19) remain linear, being slightly modified near the BZ boundaries only. The main changes are therefore reduced to a renormalization of the plasmon velocity. In Fig. 4 the dispersion curves, corresponding to quasi-momenta varying along line *1* of Fig. 3, are plotted in comparison with those for noninteracting arrays. (In all figures within this Section we use the units $\hbar = Q = v = 1$.) In what follows we use the $(j,p)$ notation for the unperturbed boson propagating along the $j$th array in the $p$th band. Then the lowest curve in Fig. 4 is, in fact, the slightly renormalized dispersion of a (2,1) boson, the middle curve describes a (1,1) boson, and the upper curve is the dispersion of a (1,2) boson. The fourth frequency, corresponding to a (2,2) boson, is far above and is not displayed in the figure. It is seen that the dis-

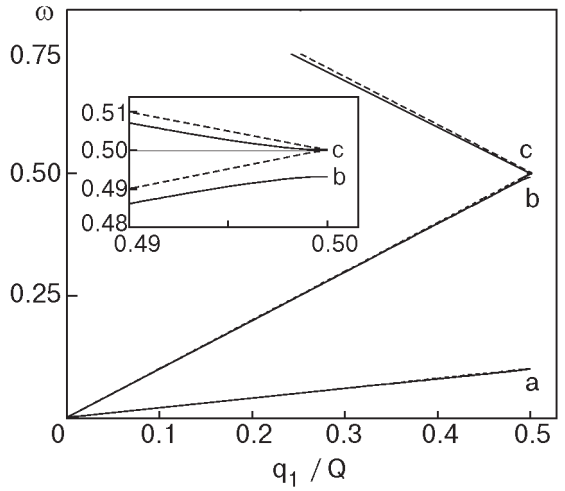


*Fig. 4.* The energy spectrum of QB (solid lines) and noninteracting arrays (dashed lines) for quasi-momenta at line *1* of Fig. 3 ($q_2 = 0.2q_1$). Points *a*, *b*, *c* on the figure correspond to the point *A* at the BZ boundary. Inset: Zoomed vicinity of the point $q_1/Q = 0.5$; $\omega = 0.5$.

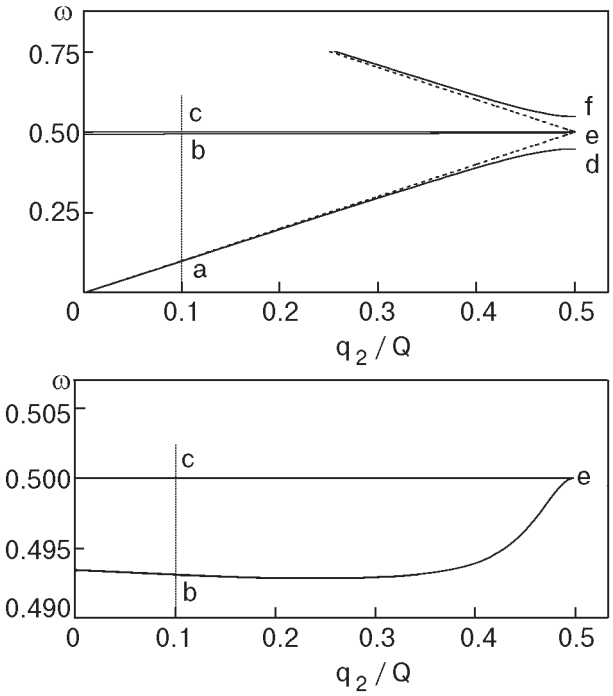


*Fig. 5.* Upper panel: The energy spectrum of QB (solid lines) and noninteracting arrays (dashed lines) for quasi-momenta at the BZ boundary (line *2* in the Fig. 3). Points *d*, *e*, *f* in the figure correspond to the corner *B* of the BZ. Lower panel: Zoomed vicinity of the line $\omega = 0.5$ .

persion remains linear along the whole line *1* except in the nearest vicinity of the BZ boundary (see inset in Fig. 4).

The interband hybridization gap for the bosons propagating along the first array can be estimated as

$$\Delta\omega_{12} \sim vQ\varepsilon\frac{r_0}{a} .$$

Similar gaps exist near the boundary of the BZ for each odd and next even energy band, as well as for each even and next odd band near the lines $q_1 = 0$ or $q_2 = 0$. The energy gap between the $p$th and $(p+1)$-th bands is estimated as

$$\Delta\omega_{p,p+1} \sim vQ\varepsilon\frac{r_0}{a}o(p^{-1}) .$$

For large enough band number $p$ interaction is effectively suppressed, $\phi_{1p2p'} \to 0$, and the gaps vanish.

Dispersion curves corresponding to quasi-momenta lying at the BZ boundary $q_1 = Q/2$, $0 \le q_2 \le Q/2$ (line *2* in Fig. 3), are displayed in Fig. 5. Again, the dispersion laws are nearly linear, and deviations from linearity are observed only near the corner of the BZ. The lowest curve describes the dispersion of the (2,1) wave. Its counterpart in the second band (2,2) is described by the highest curve in the figure. In the zero the approximation, two modes $(j,1)$ propagating along the first array are degenerate with unperturbed frequency $\omega = 0.5$. The interaction lifts the degeneracy. The lowest of two middle curves corresponds to the $(1,u)$ boson, and upper of them describes the $(1,g)$ boson. Here the indices $g$, $u$ denote a boson parity with respect to the transposition of the band numbers. Note that the $(1,g)$ boson exactly conserves its unperturbed frequency $\omega = 0.5$. The latter fact is related to the square symmetry of the QBs. The points *a*, *b*, *c* in Figs. 4 and 5 are the same.

Now consider the dispersion of modes with quasi-momenta on line *3* in Fig. 3. We start with $\mathbf{q}$ not too close to the BZ corner $q_1 = q_2 = Q/2$. In this case, the initial frequencies of modes belonging to the same band coincide, $\omega_{1p\mathbf{q}} = \omega_{2p\mathbf{q}} \equiv \omega_{p\mathbf{q}}$. Therefore the modes are strongly mixed:

$$\tilde{\theta}_{gp\mathbf{q}} = \frac{1}{\sqrt{2}}\left(1 - \frac{1}{2}\beta_{p\mathbf{q}}\right)(\theta_{2p\mathbf{q}} + \theta_{1p\mathbf{q}}) -$$

$$-\frac{1}{\sqrt{2}}\sum_{p'\neq p}(\phi_{p'p\mathbf{q}}\theta_{1p'\mathbf{q}} - \phi_{pp'\mathbf{q}}\theta_{2p'\mathbf{q}}), \qquad (25)$$

$$\tilde{\theta}_{up\mathbf{q}} = \frac{1}{\sqrt{2}}\left(1 - \frac{1}{2}\beta_{p\mathbf{q}}\right)(\theta_{2p\mathbf{q}} - \theta_{1p\mathbf{q}}) -$$

$$-\frac{1}{\sqrt{2}}\sum_{p'\neq p}(\phi_{p'p\mathbf{q}}\theta_{1p'\mathbf{q}} + \phi_{pp'\mathbf{q}}\theta_{2p'\mathbf{q}}). \qquad (26)$$

The corresponding eigenfrequencies are shifted from their bare values

$$\tilde{\omega}^2_{gp\mathbf{q}} = \omega^2_{p\mathbf{q}}\left[1 + \phi_{1p2p\mathbf{q}} + \sum_{p'\neq p}\gamma_{pp'\mathbf{q}}\right], \quad (27)$$

$$\tilde{\omega}^2_{up\mathbf{q}} = \omega^2_{p\mathbf{q}}\left[1 - \phi_{1p2p\mathbf{q}} + \sum_{p'\neq p}\gamma_{pp'\mathbf{q}}\right], \quad (28)$$

In zeroth order of perturbation theory, the modes (25), (26) have a definite $j$-parity with respect to transposition of array numbers $j = 1, 2$. Due to the repulsive character of the interaction, the odd modes $(u,p)$, $p = 1, 2$, (26) correspond to lower frequencies (28) and the even modes $(g,p)$ (25) correspond to the higher ones (27). The dispersion curves at the BZ diagonal are displayed in Fig. 6. The points $d$, $e$, and $f$ in Fig. 6 are the same as in the Fig. 5.

At the BZ corner $q_1 = q_2 = Q/2$ all four initial modes in the zeroth approximation are degenerate and have also a definite $p$-parity with respect to transposition of band numbers $p = 1, 2$. The inter-wire interaction partially lifts the degeneracy. In zeroth-order approximation, the lowest frequency corresponds to a $(g,u)$ boson, symmetric with respect to transposition of the array numbers, but antisymmetric with respect to the transposition of band numbers. The upper curve describes a $(u,u)$ boson with odd $j$-parity and $p$-parity. Degeneracy of two middle modes with even band parity, $(g,g)$ and $(u,g)$ bosons, is provided by the symmetry of interaction in a square superlattice (7). Note once more that their frequency equals to its unperturbed value $\omega = 0.5$.

All these results show that the quantum states of the 2D quantum bar conserve the quasi-1D character of the Luttinger-like liquid in the major part of momentum space, and that the 2D effects can be

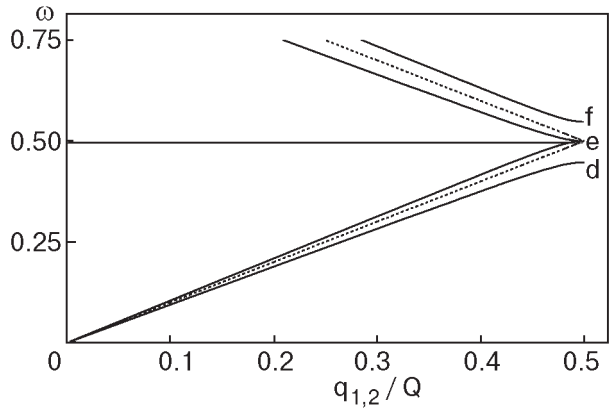


*Fig. 6*. The energy spectrum of QB (solid lines) and noninteracting arrays (dashed lines) for quasi-momenta on the diagonal of the BZ (line *3* in Fig. 3). Points $d$, $e$, $f$ in the figure correspond to corner $B$ of the BZ.

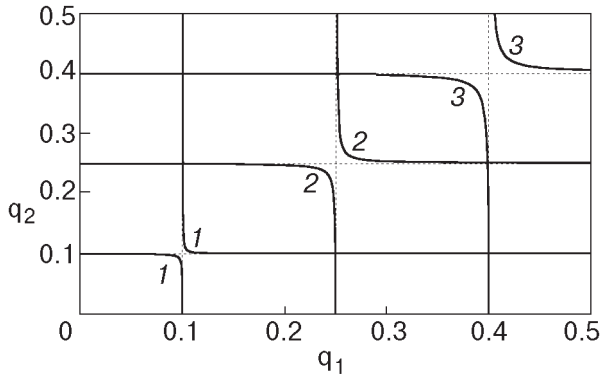


*Fig. 7*. The lines of equal frequency for QB (solid lines) and noninteracting arrays (dashed lines). Lines *1*, *2*, *3* correspond to the frequencies $\omega_1 = 0.1$, $\omega_2 = 0.25$, $\omega_3 = 0.4$.

successfully calculated within the framework of perturbation theory. However, bosons with quasi-momenta close to the diagonal of the first BZ are strongly mixed bare 1D bosons. These excitations are essentially two-dimensional, and therefore the lines of equal energy in this part of BZ are modified by the 2D interaction (see Fig. 7). It is clearly seen that deviations from linearity occur only in a small part of the BZ. The crossover from LL to FL behavior around isolated points of the BZ due to a single-particle hybridization (tunneling) for Fermi excitations was noticed in Refs. 4 and 10, where a mesh of horizontal and vertical stripes in superconducting cuprates was studied.

### 6. Correlations and observables

The structure of the energy spectrum analyzed above predetermines optical and transport properties of the QBs. Let us consider an ac conductivity whose spectral properties are given by a current—current correlator

$$\sigma_{jj'}(\mathbf{q},\omega) = \sigma'_{jj'}(\mathbf{q},\omega) + i\sigma''_{jj'}(\mathbf{q},\omega) =$$

$$= \frac{1}{\omega}\int_0^\infty dt e^{i\omega t}\left\langle [J_{j1\mathbf{q}}(t), J^\dagger_{j'1\mathbf{q}}(0)]\right\rangle .$$

Here $J_{jp\mathbf{q}} = \sqrt{2}vg\pi_{jp\mathbf{q}}$ is a current operator of the $j$th array. For simplicity we restrict ourselves to the first band. For noninteracting wires, the current—current correlator is reduced to the conventional LL expression [17],

$$\left\langle [J_{j1\mathbf{q}}(t), J^\dagger_{j'1\mathbf{q}}(0)]\right\rangle_0 = -2ivg\omega_{j1\mathbf{q}}\sin(\omega_{j1\mathbf{q}}t)\delta_{jj'}$$

with metallic Drude peak

$$\sigma'_{jj'}(\mathbf{q},\omega>0)=\pi vg\delta(\omega-\omega_{j1\mathbf{q}})\delta_{jj'}\ . \qquad (29)$$

The corresponding imaginary part contains a single pole at the resonance frequency $\omega_{j1\mathbf{q}}$,

$$\sigma'_{jj'}(\mathbf{q},\omega>0)=\frac{2vg\omega^2_{jp\mathbf{q}}}{\omega(\omega^2-\omega^2_{jp\mathbf{q}})}\,\delta_{jj'}\ .$$

For interacting wires, where $\phi_{jpj'p'\mathbf{q}}\neq 0$, the correlators may easily be calculated after diagonalization of the Hamiltonian (8) by the transformations (14) for $\mathbf{q}$ off the diagonal of the first BZ, or by the transformations (25) and (26) for $\mathbf{q}$ lying on the diagonal of the BZ.

Consider first the quasi-momenta $\mathbf{q}$ lying far from the diagonal of the first BZ. In this case, the transformations for the field momenta can be obtained in a similar manner to the transformations (14) for the field coordinates. As a result, one has:

$$\left\langle[J_{11\mathbf{q}}(t),J^{\dagger}_{11\mathbf{q}}(0)]\right\rangle=$$

$$=-2ivg(1-\beta_{1\mathbf{q}})\tilde{\omega}_{11\mathbf{q}}\sin(\tilde{\omega}_{11\mathbf{q}}t)-$$

$$-2ivg\sum_p\phi^2_{p\mathbf{q}}\tilde{\omega}_{2p\mathbf{q}}\sin(\tilde{\omega}_{2p\mathbf{q}}t)\ ,$$

$$\left\langle[J_{11\mathbf{q}}(t),J^{\dagger}_{21\mathbf{q}}(0)]\right\rangle=-2ivg\phi_{\mathbf{q}}\times$$

$$\times[\tilde{\omega}_{11\mathbf{q}}\sin(\tilde{\omega}_{11\mathbf{q}}t)-\tilde{\omega}_{21\mathbf{q}}\sin(\tilde{\omega}_{21\mathbf{q}}t)]\ ,$$

where $\beta_{p\mathbf{q}}$, $\phi_{p\mathbf{q}}$ and $\phi_{\mathbf{q}}$ are defined in Eqs. (15), (17), (18). Then, for the optical absorbtion $\sigma'$ one obtains

$$\sigma'_{11}(\mathbf{q},\omega)=\pi vg(1-\beta_{1\mathbf{q}})\delta(\omega-\tilde{\omega}_{11\mathbf{q}})+$$

$$+\pi vg\sum_p\phi^2_{p\mathbf{q}}\delta(\omega-\tilde{\omega}_{2p\mathbf{q}})\ , \qquad (30)$$

$$\sigma'_{12}(\mathbf{q},\omega)=\pi vg\phi_{\mathbf{q}}[\delta(\omega-\tilde{\omega}_{11\mathbf{q}})-\delta(\omega-\tilde{\omega}_{21\mathbf{q}})]\ . \qquad (31)$$

The longitudinal optical absorbtion (30) (i.e. the conductivity within a given set of wires) has its main peak at frequency $\tilde{\omega}_{11\mathbf{q}}\approx v|q_1|$, corresponding to the first band of the pertinent array, and an additional weak peak at the frequency $\tilde{\omega}_{21\mathbf{q}}\approx v|q_2|$, corresponding to the first band of a complementary array. It contains also a set of weak peaks at frequencies $\tilde{\omega}_{2p\mathbf{q}}\approx[p/2]\,vQ$ ($p=2,3,\ldots$) corresponding to the contribution from the higher bands of the complementary array. At the same time, a second observable becomes relevant, namely, the transverse optical conductivity (31). It is proportional to the interaction strength and has two peaks at frequencies $\tilde{\omega}_{11\mathbf{q}}$ and $\tilde{\omega}_{21\mathbf{q}}$ in the first bands of both sets of wires. For $|\mathbf{q}|\to 0$ Eq. (30) reduces to that for an array of noninteracting wires (29), and the transverse optical conductivity (31) vanishes.

In the case when the quasi-momenta $\mathbf{q}$ belong to the diagonal of the first BZ, the transformations for the field momenta are similar in form to Eqs. (25) and (26). The current–current correlation functions have the form

$$\left\langle[J_{11\mathbf{q}}(t),J^{\dagger}_{11\mathbf{q}}(0)]\right\rangle=-ivg(1-\beta'_{1\mathbf{q}})\times$$

$$\times[\tilde{\omega}_{g1\mathbf{q}}\sin(\tilde{\omega}_{g1\mathbf{q}}t)+\tilde{\omega}_{u1\mathbf{q}}\sin(\tilde{\omega}_{u1\mathbf{q}}t)]-$$

$$-ivg\sum_{p\neq 1}\phi^2_{p\mathbf{q}}\tilde{\omega}_{p\mathbf{q}}\sin(\tilde{\omega}_{p\mathbf{q}}t)\ ,$$

$$\left\langle[J_{1\mathbf{q}}(t),J^{\dagger}_{2\mathbf{q}}(0)]\right\rangle=$$

$$=-ivg[\tilde{\omega}_{g1\mathbf{q}}\sin(\tilde{\omega}_{g1\mathbf{q}}t)-\tilde{\omega}_{u1\mathbf{q}}\sin(\tilde{\omega}_{u1\mathbf{q}}t)]$$

with $\omega_{p\mathbf{q}}$ and $\beta'_{p\mathbf{q}}$ defined by Eqs. (3), (18), and the optical conductivity is estimated as

$$\sigma'_{11}(\mathbf{q},\omega>0)=\frac{\pi vg}{2}(1-\beta'_{1\mathbf{q}})\times$$

$$\times[\delta(\omega-\tilde{\omega}_{q1\mathbf{q}})+\delta(\omega-\tilde{\omega}_{u1\mathbf{q}})]+$$

$$+\pi vg\sum_{p\neq 1}\phi^2_{p\mathbf{q}}\delta(\omega-\omega_{p\mathbf{q}})\ , \qquad (32)$$

$$\sigma'_{12}(\mathbf{q},\omega>0)=\frac{\pi vg}{2}[\delta(\omega-\tilde{\omega}_{q1\mathbf{q}})-\delta(\omega-\tilde{\omega}_{u1\mathbf{q}})]\ . \qquad (33)$$

The longitudinal optical conductivity (32) has a split double peak at frequencies $\tilde{\omega}_{11\mathbf{q}}$ and $\tilde{\omega}_{21\mathbf{q}}$, instead of a single peak. Again, a series of weak peaks occurs at frequencies $\omega_{p\mathbf{q}}$ corresponding to contributions from higher bands $p=2,3,4,\ldots$ The transverse optical conductivity (33), similarly to the nondiagonal case (31), has a split double peak at frequencies $\tilde{\omega}_{11\mathbf{q}}$ and $\tilde{\omega}_{21\mathbf{q}}$.

The imaginary part of the ac conductivity $\sigma''_{jj'}(\mathbf{q},\omega)$ is calculated within the same approach. Its longitudinal component for $\mathbf{q}$ far from the BZ diagonal equals

$$\sigma''_{11}(\mathbf{q},\omega)=2vg\frac{\omega^2_{11\mathbf{q}}}{\omega}\left[\frac{1-\beta_{1\mathbf{q}}}{\omega^2-\tilde{\omega}^2_{11\mathbf{q}}}+\sum_p\frac{\phi^2_{p\mathbf{q}}}{\omega^2-\tilde{\omega}^2_{2p\mathbf{q}}}\right].$$

Beside the standard pole at zero frequency and the main pole at the resonance frequency $\omega_{11\mathbf{q}}$, the real part has an additional series of high-band satellites. The corresponding expression for $\sigma''_{22}(\mathbf{q},\omega)$ can be obtained after the replacement $1\leftrightarrow 2$. For quasi-

momenta at the diagonal, the longitudinal optical absorption is

$$\sigma''_{11}(\mathbf{q},\omega) = (1-\beta_{1\mathbf{q}})\frac{vg}{\omega}\left[\frac{\tilde{\omega}^2_{g1\mathbf{q}}}{\omega^2-\tilde{\omega}^2_{g1\mathbf{q}}}+\frac{\tilde{\omega}^2_{u1\mathbf{q}}}{\omega^2-\tilde{\omega}^2_{u1\mathbf{q}}}\right]+$$

$$+\,2vg\,\frac{\omega^2_{1\mathbf{q}}}{\omega}\sum_{p=1}^{\infty}\frac{\phi^2_{p\mathbf{q}}}{\omega^2-\omega^2_{p\mathbf{q}}}\,.$$

It contains two main poles similar to two peaks in the optical conductivity, and the series of poles contributed by the higher bands. The transverse component of the imaginary part of the ac conductivity has the same form for any $\mathbf{q}$:

$$\sigma''_{12}(\mathbf{q},\omega) = 2vg\phi_{\mathbf{q}}\omega\left[\frac{1}{\omega^2-\tilde{\omega}^2_{u1\mathbf{q}}}-\frac{1}{\omega^2-\tilde{\omega}^2_{g1\mathbf{q}}}\right].$$

It always contains two poles and vanishes for noninteracting wires.

One of the main effects specific for a QB is the appearance of a nonzero transverse momentum – momentum correlation function. In space–time coordinates $(\mathbf{x},t)$ its representation reads

$$G_{12}(\mathbf{x},t) = \left\langle[\pi_1(x_1,0;t),\pi_2(0,x_2;0)]\right\rangle. \quad (34)$$

This function describes the momentum response at the point $(0,x_2)$ of the second array at the moment $t$ caused by initial $(t=0)$ perturbation at the point $(x_1,0)$ of the first array. Standard calculations similar to those described above lead to the following expression:

$$G_{12}(\mathbf{x},t) = -i\,\frac{V_0 r_0^2}{4\pi^2\hbar v}\int_{-\infty}^{+\infty}dk_1dk_2\Phi_{k_1k_2}\times$$

$$\times\sin(k_1x_1)\sin(k_2x_2)\,\frac{k_2\sin(k_2vt)-k_1\sin(k_1vt)}{k_2^2-k_1^2}. \quad (35)$$

Here $\Phi_{k_1k_2}$ is defined by Eq. (11) with $p=p_1$, $p'=p_2$, and $k_{1,2}$ from Eq. (23).

This correlator is shown in Fig. 8. Here the nonzero response corresponds to the line determined by the obvious kinematic condition $|x_1|+|x_2|=vt$. The finiteness of the interaction radius slightly spreads this peak and changes its profile.

## 7. Conclusion

In conclusion, we have demonstrated that the energy spectrum of QBs shows the characteristic properties of LL at $|q|,\omega\to 0$, but at finite $\mathbf{q}$, the density and momentum waves may have either 1D or 2D character depending on the direction of the wave vector. Due to an interwire interaction, unperturbed states propagating along the two arrays are always mixed, and the transverse components of the correlation functions do not vanish. For quasimomentum lying on the diagonal of the BZ, such mixing is strong, and the transverse correlators have the same order of magnitude as the longitudinal ones.

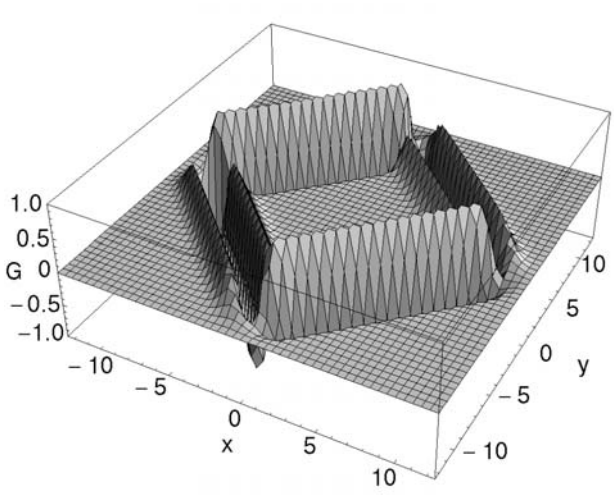


*Fig. 8.* The transverse correlation function $G_{12}(x_1,x_2;t)$ for $r_0=1$ and $vt=10$.

**Acknowledgement**

S. G. and K. K. are indebted to L. Gorelik, M. Jonson, I. Krive, and R. Shekhter for helpful discussions. They also thank Chalmers Technical University, where this work was started, for hospitality and support. This research is supported in part by grants from the Israel Science foundations, the DIP German–Israel cooperation program, and the USA–Israel BSF program. S. G. is happy to see this paper published in the special issue devoted to the Jubilee of his old friend and colleague, Academician Victor Eremenko.

1. P. W. Anderson, *Science* **235**, 1196 (1987).
2. J. E. Avron, A. Raveh, and B. Zur, *Rev. Mod. Phys.* **60**, 873 (1988).
3. Y. Avishai and J. M. Luck, *Phys. Rev.* **B45**, 1074 (1992).
4. F. Guinea and G. Zimanyi, *Phys. Rev.* **B47**, 501 (1993).
5. V. Emery, E. Fradkin, S. A. Kivelson, and T. C. Lubensky, *Phys. Rev. Lett.* **85**, 2160 (2000).
6. A. Vishwanath and D. Carpentier, *Phys. Rev. Lett.* **86**, 676 (2001).

7. J. Silva-Valencia, E. Miranda, and R. R. dos Santos, *cond-mat/0107114*.
8. R. Mukhopadhyay, C. L. Kane and T. C. Lubensky, *Phys. Rev.* **B63**, 081103(R) (2001); *cond-mat/0102163*.
9. C. S. Hern, T. C. Lubensky, and J. Toner, *Phys. Rev. Lett.* **83**, 2745 (1999).
10. A. H. Castro Neto and F. Guinea, *Phys. Rev. Lett.* **80**, 4040 (1998).
11. R. Egger, A. Bachtold, M. S. Fuhrer, M. Bockrath, D. H. Cobden, and P. L. McEuen, *cond-mat/0008008*.
12. T. Rueckes, K. Kim, E. Joselevich, G. Y. Tseng, C.-L. Cheung, and C. M. Lieber, *Science* **289**, 94 (2000).
13. J. von Delft and H. Schoeller, *Ann. Physik* **7**, 225 (1998).
14. K. Sasaki, *cond-mat/0112178*.
15. S. G. Louie: in: *Carbon Nanotubes*, M. S. Dresselhaus, G. Dresselhaus, and Ph. Avouris (eds.), *Topics Appl. Phys.* **80**, 113 (2001), Springer, Berlin 2001.
16. H. Ajiki and T. Ando, *J. Phys. Soc. Jpn.* **65**, 505 (1996).
17. J. Voit, *Rep. Prog. Phys.* **58**, 977 (1994).